



Experimental and theoretical comparative analysis of pure WO_3 and La doped WO_3 for degradation of MB

Ayesha Younas¹ · Tahir Iqbal¹ · Abdullah Almohammed² · Sumera Afsheen³

Received: 12 August 2023 / Accepted: 15 September 2023 / Published online: 17 October 2023
© The Author(s), under exclusive licence to Springer Science+Business Media, LLC, part of Springer Nature 2023

Abstract

This study reports the simple synthesis of pure and La-doped (1, 2, 3, 4 and 5%) WO_3 nanoparticles (NPs) for the degradation of MB dye. The UV–Vis, XRD, FTIR, SEM and PL techniques have been utilized for the evaluation of prepared samples. The photo catalytic activity of these synthesized samples has been observed for the degradation of methylene blue (MB) in the presence of visible light via photo catalysts (WO_3 , La- WO_3) NPs. Additionally, the suppression of the band gap from 2.81 to 2.23 eV along photo generated electron–hole pair has been demonstrated by UV visible and PL spectroscopy respectively. The crystalline size of 4% La- WO_3 , reduced from 30 to 11 nm as compared to pure WO_3 . FTIR spectroscopy analysis reveals the synthesized material is composed of tungsten and oxygen. However, in the presence of visible light, the optimal 4% La-doped WO_3 NPs' are capable of degrade methylene blue (MB) to 94% within 180 min. To test the stability of the optimized catalyst, reusability and trapping tests have been conducted. The correlation between the theoretical model and the experiments has also been performed using the COMSOL Multiphysics module 5.3a.

Keywords Tungsten trioxide (WO_3) · Methylene blue (MB) · La-doped WO_3 · COMSOL · Photo catalysis

Ayesha Younas, Tahir Iqbal · Abdullah Almohammed and Sumera Afsheen have contributed equally.

✉ Ayesha Younas
21011710-025@uog.edu.pk

✉ Tahir Iqbal
tahir.awan@uog.edu.pk

✉ Abdullah Almohammed
arda@iu.edu.sa

Sumera Afsheen
sumera.afsheen@uog.edu.pk

¹ Department of Physics, Faculty of Science, University of Gujrat, Hafiz Hayat Campus, Gujrat 50700, Pakistan

² Department of Physics, Faculty of Science, Islamic University of Madinah, Madinah 42351, Saudi Arabia

³ Department of Zoology, Faculty of Science, University of Gujrat, Hafiz Hayat Campus, Gujrat 50700, Pakistan

1 Introduction

Water is the basic need of all living organisms as they can't survive without it. Fresh and clean water is being used in homes and industries as well as for domestic purposes. Water pollution has become a major problem of the world and it is caused by the daily activities of humans, the usage of organic dyes and industrial effluents (Chaudhry and Malik 2017; Haseena 2017). According to careful estimation, 20% of dyes used in the textile industry each year, including Thymol blue, Rhodamine blue, Indigo Red, Victoria blue, MB and Eriochrome etc. are released in wastewater (Jabbar and Graimed 2022; Al-Nuaim et al. 2023; Villar et al. 2022; Mutahir et al. 2022). The production of crops is abolished by water pollution; viruses, bacteria and parasites are affecting both human and aquatic life (Haseena 2017; Antony et al. 2021). Therefore, a sufficient method is necessary for the purification of contaminated water (Azimi et al. 2017).

Photocatalysis can perfectly mineralize the contaminants and is considered to be the best method for treating wastewater (Koe et al. 2020; Chen et al. 2020). Numerous photocatalytic materials, including TiO_2 , Bi_2O_3 , ZnO and WO_3 (Martínez et al. 2011; Ullah and Dutta 2008; Chen et al. 2015) have been studied in recent years and several redox reactions take place at photocatalyst's surface (Štengl et al. 2009).

Tungsten trioxide (WO_3) has gained much attention because it has a strong ability to break down contaminants, long lifetime, non-hazardous and cost effective (Ren et al. 2021). It is a semiconductor material that has an indirect band gap that reacts with visible light and its band gap energy is less than TiO_2 (Iqbal et al. 2022a; Li et al. 2013). Visible light is better absorbed by WO_3 due to its small band gap (Ahmed and Haider 2018). Additionally, it has chemical properties that are stable in aqueous solution (Zhu et al. 2017a). The valence band energy for the oxidation reaction and the conduction band energy for reduction is not sufficient to employ O_2 as an acceptor of electrons. Therefore, the band gap of WO_3 is not highly suitable for organic breakdown under UV or visible light. This led to several investigations being done to alter the structure of WO_3 by doping and composites with other transition metals and semiconductor materials. (Zhu et al. 2017a; Iqbal et al. 2022b; Pal et al. 2018; Han et al. 2020).

By changing the material's physical and optical properties, rare-earth metal doping such as (lanthanum, cerium & neodymium) transition metals or noble metal doping such as (rhodium, silver, platinum and gold) are capable of improving a semiconductor's photocatalytic efficiency (Shandilya et al. 2022). Lanthanides have half-filled f orbitals that could act as electron and hole acceptors and cause an optical absorption redshift. In addition, the narrow band gap facilitates charge separation and it is a crucial aspect of rare-earth doping (Murillo-Sierra, et al. 2021) Tahir Iqbal, et al., reported that La-doped CuO NPs were prepared by using green method for the degradation of MB dye (Lan et al. 2014). La doping reduces the recombination rate of electron hole pair and decreases the crystallite size of CuO NPs that exhibit 84% degradation efficiency. It reveals that modified samples respond as an efficient photocatalyst (Zhu et al. 2017b).

In this study, a facile hydrothermal method has been used for the preparation of La-doped (1, 2, 3, 4 & 5%) WO_3 NPs for the photodegradation of methylene Blue (MB) and this method is cost-effective, simple and easier to use than other methods. The novel aspect of this research is that it provides a comparative analysis of pure and La-doped WO_3 by using experimental and theoretical simulation. In addition, by using RF module of COMSOL Multiphysics 5.3a the degradation of MB was studied which is well correlated with experimental results that has been used to examine the photocatalytic performance of the

La-doped WO_3 nanoparticles. This article will discuss the photocatalytic degradation of MB dye by using synthesized nanoparticles in the presence of visible light.

2 Materials and methods

2.1 Material used

In order to synthesize tungsten oxide (WO_3) and La-doped WO_3 nanoparticles, sodium tungstate dihydrate ($\text{Na}_2\text{WO}_4 \cdot 2\text{H}_2\text{O} \geq 99\%$), distilled (DI) water, hydrochloric acid ($\text{HCl} \geq 99\%$), Lanthanum nitrate hexahydrate ($\text{La}(\text{NO}_3)_3 \cdot 6\text{H}_2\text{O} \geq 99\%$) and Ethanol ($\text{C}_2\text{H}_6\text{O}$) were used as raw materials and precursors. The entire set of materials and precursors needed for the current experiment was purchased from the Sigma Aldrich company.

2.1.1 Pure WO_3 and La doped WO_3 synthesis

A hydrothermal method was used for the fabrication of pure WO_3 and La doped (1, 2, 3, 4 & 5%) WO_3 NPs. The pure WO_3 is prepared by mixing 2 g of Sodium tungstate dihydrate in 80 ml distilled water as shown in (Fig. 1). The mixture continuously stirred for 30 min at 1500 rpm by adding few drops of HCl until its pH become 3. In Teflon lined stainless steel autoclave, the entire solution was added and placed in an oven for 24 h. After that, the prepared precipitates were washed with ethanol (20 ml) and distilled water (20 ml) to maintain the PH of the solution. The entire precipitates were dried at 120 °C for 24 h in an oven and calcinated at 550 °C for 120 min thus the powdered material of nanoparticles was obtained. In order to synthesize La-doped WO_3 NPs, the concentration of precursors is varied. For 1% La-doped WO_3 NPs, 1.98 g of $\text{Na}_2\text{WO}_4 \cdot 2\text{H}_2\text{O}$ were dissolved in 80 ml distilled water and 0.02 g of $\text{La}(\text{NO}_3)_3 \cdot 6\text{H}_2\text{O}$ were added into the entire solution. Similar to this, 0.04, 0.06, 0.08 and 0.10 g of La dopant were added in 1.96, 1.94, 1.92 and 1.9 g of $\text{Na}_2\text{WO}_4 \cdot 2\text{H}_2\text{O}$, respectively, for 2, 3, 4 and 5% La-doped WO_3 NPs, while the remaining procedure remains same.

2.2 Characterization of photocatalysts

In this research work, various characterization techniques were used to examine the synthesized nanomaterials. such as X-rays diffraction (XRD) spectroscopy (JDX-3532) was used to calculate crystalline size of material and Scanning Electron Microscopy (JSM-IT-100) was used to analyze the morphology of material. However, UV–vis double beam Spectroscopy (Double Beam UV–Vis Spectrophotometer SP-IUV&, UOG) and Photoluminescence (PL) spectroscopy (FP-8200 Spectrofluorometer JASCO) were used to evaluate the bandgap and Photoluminescence behavior of fabricated nanomaterials. To identify elemental composition, FTIR spectroscopy is used. At last, the photocatalytic activity was measured by using photocatalytic reactor (TECHNISTRO) of all fabricated materials.

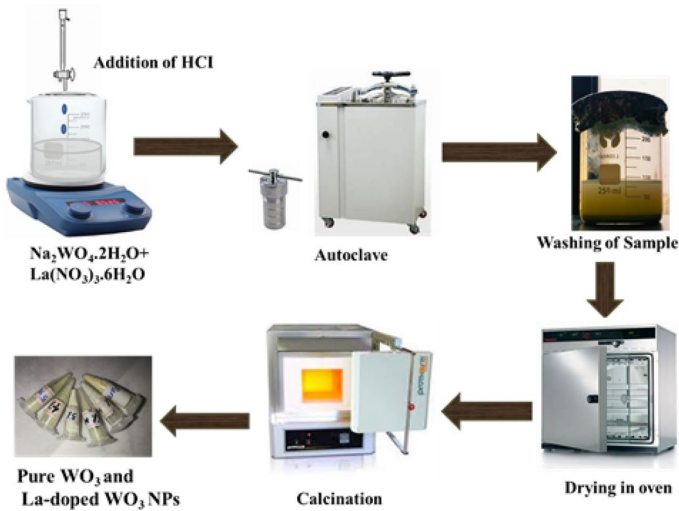


Fig. 1 Schematic representation of the preparation of pure and La-doped WO_3 NPs

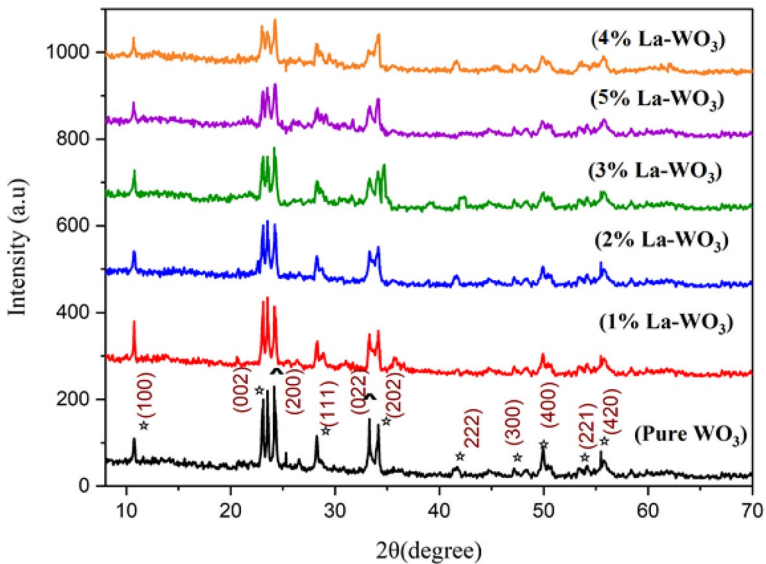


Fig. 2 XRD pattern of pure WO_3 and La-doped WO_3 NPs

3 Results and discussion

3.1 Structural analysis (X-ray diffraction)

X-ray diffraction (XRD) technique were used to examine the structural properties as well as the average crystallite size of synthesized nanoparticles. X-ray diffraction pattern of Pure WO_3 and La-doped (1, 2, 3, 4 & 5%) WO_3 NP's results were shown in Fig. 2.

Fig. 3 Peak shift of pure WO₃ and La-doped WO₃ NPs

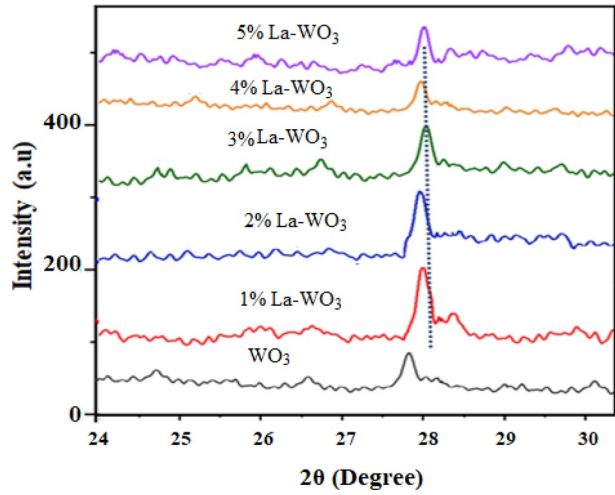


Table 1 Crystallite size of Pure and doped WO₃ by XRD analysis and band gap energy by UV–Vis analysis

Sample	2θ	FWHM (Deg)	Crystallite size (nm)	Band gap (eV)
Pure WO ₃	28.09	0.244	30	2.81
1% La-WO ₃	28.11	0.241	27	2.74
2% La-WO ₃	28.14	0.239	22	2.6
3% La-WO ₃	28.15	0.232	19	2.49
4% La-WO ₃	28.17	0.229	11	2.23
5% La-WO ₃	28.19	0.226	15	2.39

The typical hexagonal wurtzite structure of Pure WO₃ NPs showed peaks positioned at 2θ values of 23.31°, 24.27°, 28.30°, 33.34°, 41.61°, 54.68° and 55.76°, which are indexed as (100), (002), (200), (111), (222), (400) and (221) planes, respectively. The average crystallite size of La-doped (1, 2, 3, 4 &5%) WO₃ NPs decreased by increasing the amount of Lanthanum.

The prepared samples are extremely crystalline because the dopant has not distorted the crystal atom. By increasing the doping concentration, the planes of XRD also slightly moved towards a higher angle, showing the presence of La in the WO₃ lattice and the intensity of peaks decreases which often correspond with smaller particle sizes (Munawar et al. 2023a) as shown in Fig. 3. The difference in ionic radius between La³⁺ and W⁶⁺ may be responsible for this shift (Fatima et al. 2023). The band gap energy and crystalline size of all catalysts listed in Table 1. The Debye–Scherrer Eq. (1) was used to calculate the crystallite size of prepared NPs (Jeevitha et al. 2018; Deshmane et al. 2015).

$$D = \frac{0.89\lambda}{\beta \cos \theta} \tag{1}$$

where D is the measurement of the crystallite size of material, λ is the measurement of the radiation’s wavelength, β is the measurement of the full width half maximum (FWHM) and θ represents the diffraction angle (Maryam 2023). The high intense peak is used to calculate

the FWHM and the average crystallite size is also calculated using the Debye–Scherrer formula. The Eq. (2) is used to calculate the lattice parameters (Chandekar et al. 2020).

$$\frac{1}{d_{(hkl)}^2} = \frac{4}{3} \left[\frac{h^2 + hk + k^2}{a^2} \right] + \frac{l^2}{c^2} \quad (2)$$

The lattice parameters “a and c” of doped WO₃ are smaller than pure WO₃ as shown in Table 2. There is no remarkable change in the values of c/a, proving that La does not alter the crystal structure of pure WO₃. It’s important to note that the incorporation of La is responsible for the deformation of the WO₃ and it stores microstrain energy (Munawar et al. 2023b) which is calculated by using Eq. 3.

$$\delta = \frac{1}{D^2} \quad (3)$$

The microstrain values rise by changing the concentration of La (1–5%) in WO₃ lattice. The presence of defects might facilitate charge carrier separation more quickly and enhanced photocatalytic efficiency.

3.2 Morphological and elemental analysis

The Scanning electron microscopy (SEM) of pure WO₃ and 3% La-WO₃ NPs with different magnifications are shown in Fig. 4a, c and b, d respectively. WO₃ powder has small particle size and has an irregular roughly nano-spheroid structure with a minor agglomeration. The size of nanoparticles lies in the range of 30–40 nm. The La doped WO₃ nanoparticles causes defect sites and surface disorder, hence it is expected that La doped (1, 2, 3, 4 & 5%) WO₃ nanoparticles have more pores size than WO₃ samples. When 3% La-doped WO₃ is compared to pure WO₃ at the same resolution and magnification, the doping material is distinguishable (Khan et al. 2021). This ultimately leads to an increase in the porosity of synthesized nanoparticles. The presence of La ions in the WO₃ lattice also changes the morphology of pure WO₃. The breakdown of organic contaminants in wastewater has been facilitated by these doped agglomerations. The EDX plots include the weight and molarity percentage of the pure and La-doped WO₃ as shown in Fig. 5a and b.

Table 2 The structural parameters of Pure and La-doped WO₃ NPs

Photocatalysts	Lattice constants (a=b)	c	c/a	Crystallite size (nm)	Microstrains (ε)
Pure WO ₃	7.3142	3.9189	0.5357	30	0.0011
1% La-WO ₃	7.2762	3.8982	0.5357	27	0.0013
2% La-WO ₃	7.2732	3.7871	0.5271	22	0.0020
3% La-WO ₃	7.2874	3.8523	0.5286	19	0.0027
4% La-WO ₃	7.0431	3.8024	0.5398	11	0.0082
5% La-WO ₃	7.2489	3.8567	0.5320	15	0.0040

Table 3 Comparison of current research work with previous similar studies

Sr. No	Photocatalyst	Methods	Contaminants	Degradation (%)	References
1	Mn/WO ₃	Microwave irradiation method	MB	79	Sayed Abhudhahir and Kandasamy (2015)
2	Ag/WO ₃	Microwave irradiation method	MB	81	Mohammed Harshulkhan, et al. (2016)
3	Cu/WO ₃	Chemical	Tetracycline (TC)	93.7	Quyen et al. (2021)
4	Ta/ WO ₃	Hydrothermal	MB	91	Maryam et al. (2023)
5	La/ WO ₃	Hydrothermal	MB	94	Current research work

3.3 FTIR analysis

Pure and La-doped WO₃ nanomaterials at different concentrations of 1, 2, 3, 4, and 5%, respectively, were determined in the range of 500–4000 cm⁻¹ in FTIR spectra analysis as shown in Fig. 6. It is divided into three regions: a broad band between 1600–3700 cm⁻¹ shows two sharp peaks at 1552 and 3662 cm⁻¹. The peak at 3662 cm⁻¹ is related to the W–OH stretching mode because of the adsorption of water molecule and 1552 cm⁻¹ is due to stretching vibration of H–O–H. (Pang et al. 2012). FTIR spectra in the region of 500–900 cm⁻¹ is used to detect the changes in structure of tungsten–oxygen by varying concentration of Lanthanum. The bend at 660 cm⁻¹ was attributed to the stretching and bending vibrations for W–O–W in WO₃. The absorption band exhibits O–H stretching–bend at 1326 cm⁻¹ for WO₃.

3.4 UV–Vis absorption analysis

The optical properties of WO₃ and La doped (1, 2, 3,4 & 5%) WO₃ NPs were examined by UV–Vis absorption spectroscopy. The UV–visible tauc plot of pure WO₃ and La doped WO₃ NPs is shown in Fig. 7. The band gap energy were calculated by using Eq. 4 (Wei et al. 2016).

$$(\alpha h\nu) = C(h\nu - E_g)^{1/2} \quad (4)$$

Here, C is constant and the incident photon energy and band gap energy is represented by $h\nu$ and E_g respectively. The La-doped WO₃ nanoparticles exhibit significant light absorbance in the visible region. Band gap consistently decreases 2.81 to 2.23 eV with increasing dopant concentration. The calculated band gaps for pure WO₃ and La doped (1, 2, 3, 4 and 5%) WO₃ NPs were 2.81 2.7, 2.6, 2.49, 2.23 eV, and 2.39 eV respectively. By increasing the concentration of dopant, the band gap energy as well as crystallite size decreased. It is evident from the values of bandgap that increasing dopant concentration band gap is decreasing. But in the case of La-doped WO₃ this is limited to the 4% only. At 5% La-doped WO₃ band gap again starts to increase. This is related to the Burstein-Moss effect, which states that for a certain concentration of

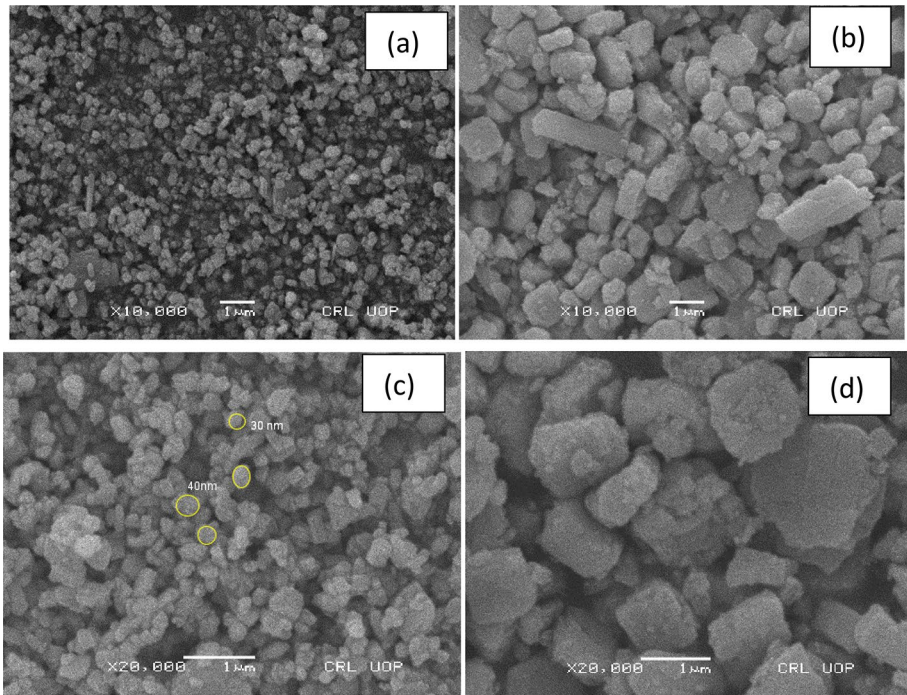


Fig. 4 SEM images of **a, c** represents pure WO_3 and **b, d** represents 3% La-doped WO_3 NPs with different magnification

impurity atoms, the fermi energy level shifts toward the valence band, resulting in a blue shift, and expands the visible bandgap of the semiconductor material. (Maryam et al. 2023). The 4% La-doped WO_3 NPs absorb more visible light because their band-gap energy values are lower than pure WO_3 NPs and hence more efficient (Govindaraj et al. 2022).

3.5 PL spectra analysis

The recombination rate of electron hole (e^-h^+) pair of a semiconducting materials is typically studied by Photoluminescence (PL) spectroscopic analysis. PL intensity peaks decrease by increasing dopant concentration. (Wei et al. 2016; He et al. 2014). The 4% La doped WO_3 NPs has lowest PL intensity, demonstrating that the presence of defects and oxygen vacancies, makes it easier for charge carriers to split apart after recombination (He et al. 2014). At 5% La concentration, PL intensity again starts to increase. This is attributed to the Burstein-Moss shift. It refers to the enhancement of the optical band gap in n-type metal oxide semiconductors as a consequence of an increase in the dopant concentration or oxygen defects (Paik et al. 2018). Figure 8. Shows the PL spectra of WO_3 and La doped

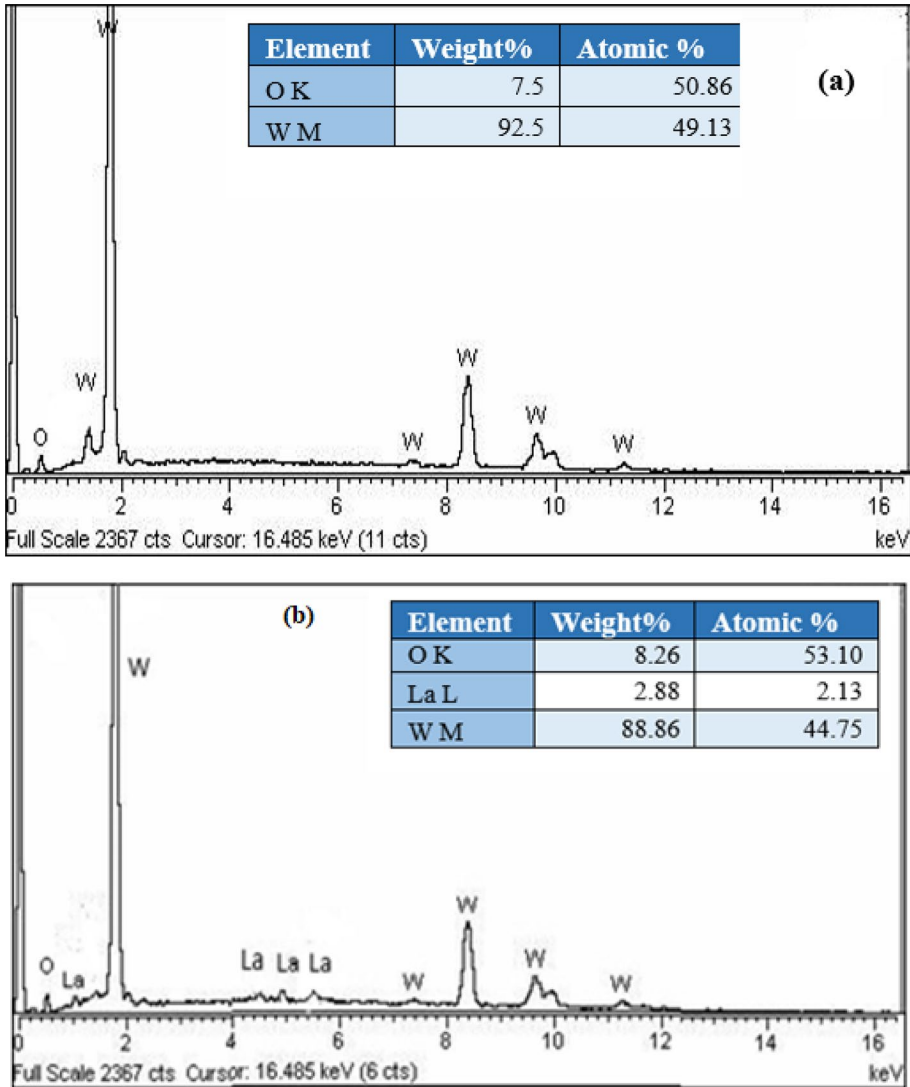


Fig. 5 a shows EDX analysis of pure WO_3 and b shows 3% La- WO_3 along with molar and weight percentage

(1, 2, 3, 4 & 5%) WO_3 NPs at 360 nm excitation wavelength. The band gap values were determined by wavelength peak at 442 nm, which correlates with UV–visible spectroscopy. The results clearly demonstrate that doping may decrease electron–hole pair recombination, resulting in greater charge carriers and ultimately increasing the degradation of contaminants. The 4% La doped WO_3 shows maximum reduction in the rate of charge carrier recombination, which is crucial for photo catalytic activity (Fig. 8).

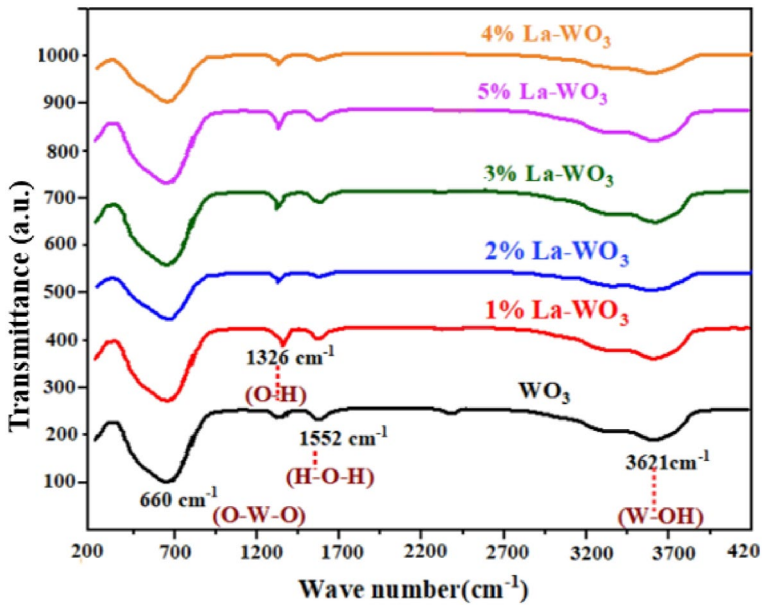
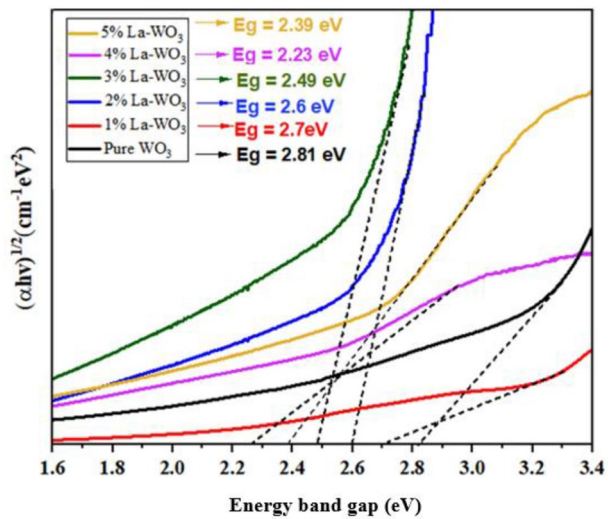


Fig. 6 FTIR spectra of pure WO_3 and La-WO_3 NPs (1%, 2%, 3%, 4% & 5%)

Fig. 7 WO_3 and La-doped WO_3 NPs (1%, 2%, 3%, 4% & 5%) of UV-Vis spectroscopy tauc plot



4 Photo catalytic activity

The Methylene blue (MB) degradation has been evaluated to determine the efficiency of the synthesized material in the presence of visible light as depicted in (Fig. 9). A 500 W tungsten-halogen lamp provided visible light irradiation and the light source's

wavelength was greater than 400 nm and its maximum operating temperature is 1000 °C. The solution of MB dye was prepared and kept in a photo catalytic reactor.

The MB dye solution is made by adding 10 mg dye in 1000 ml distilled water and the adsorption desorption equilibrium is achieved in such a way that the contaminated solution is initially stirred in the dark for approximately 30 min by adding 0.1 g/L catalyst before exposing to light (Masood 2023). The UV–Visible spectroscopy tells us the degradation by calculating the value of absorption of all samples (pure and doped) after every 30 min (Masood 2023). Firstly, we calculate the degradation efficiency with respect to time for all the prepared nanoparticles (Kannan et al. 2020). A 5 ml sample from the prepared solution was taken after every 30 min to examine the absorbance and degradation activity against particular photo catalyst.

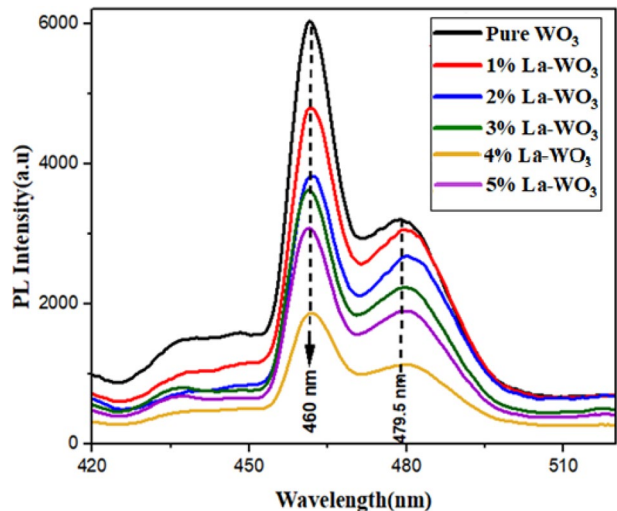
The degradation of the methylene blue (MB) dye evaluates the photo-catalytic efficiency of the synthesized nanoparticles. The efficiency of a sample is calculated using the equation below.

$$\text{Degradation (\%)} = \left(1 - \frac{C}{C_0}\right) \times 100 \tag{5}$$

The 4% La doped WO₃ NPs shows 94% degradation of MB dye within 180 min as shown in Fig. 9b. The WO₃ sample has been able to decompose only a small amount of Methylene blue, because of their larger band gap and higher electron/hole pair recombination rate (Sa-nguanprang et al. 2020). However, an impurity of transition metal (Lanthanum) has been doped in WO₃ lattice to eliminate these difficulties and the degradation efficiency of the prepared photo catalyst was enhanced by increasing the dopant concentration (Ashraf et al. 2023). The absorption intensity of MB dye decreases with increasing light exposure time and 4% La doped WO₃ NPs exhibit higher photo degradation than other fabricated catalysts (Sarojini et al. 2023).

The rate constant “k” values of MB dye degradation were 0.0014, 0.0018, 0.0022, 0.0026, 0.0040 and 0.0032 min⁻¹ for pure WO₃ and La (1, 2, 3, 4 and 5%) doped WO₃ NPs, accordingly, as depicts in Fig. 9d. The 4% La-WO₃ NPs have highest rate constant value, and it is obviously higher than those for other synthesized nanoparticles.

Fig. 8 PL spectra of WO₃ and La-WO₃ NPs (1%,2%,3%,4%& 5%)



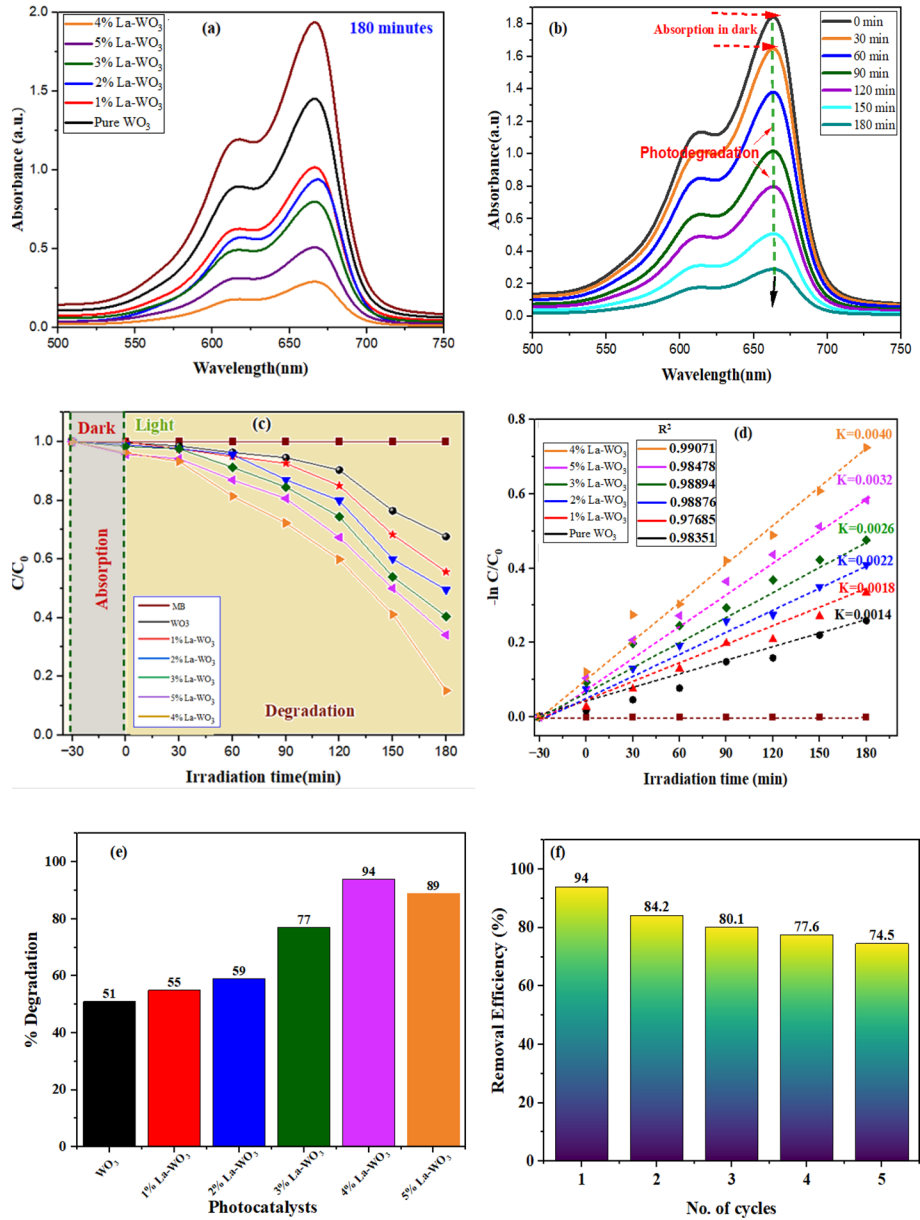


Fig. 9 **a** Photocatalytic activity of WO₃ & La doped WO₃ NPs (1%, 2%, 3%, 4% and 5%) using Methylene Blue dye at 180 min, **b** Photocatalytic activity of Methylene Blue dye of 4% La doped WO₃, **c** Photocatalytic degradation of all fabricated samples, **d** Time and $\ln[C/C_0]$ for first order kinetics of MB dye of WO₃ and La-WO₃ NPs (1%, 2%, 3%, 4% and 5%), **e** Percentage WO₃ efficiency of degradation and doping with La (1%, 2%, 3%, 4% and 5%), **f** Stability & reusability after five number of cycles of 4% La doped WO₃ for MB. (g,h) Values of Rate constants and correlation coefficient (R²)

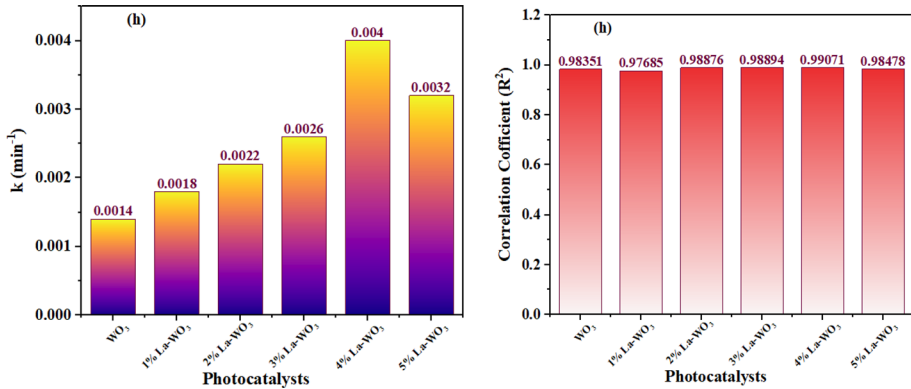


Fig. 9 (continued)

The comparison of current research work with previous reported studies mentioned in Table 3.

4.1 Kinetics of reaction

A photo catalysis is a reaction of pseudo-first order. MB dye degradation by using all synthesized catalysts were shown in Fig. 9c. Photo catalytic degradation of first order kinetics for each experiment was determined by using Eq. 6 (Weber et al. 2012).

$$\ln \left(\frac{C}{C_0} \right) = kt \tag{6}$$

“C” shows specific concentration with variation in time (t), maximum concentration “ C_0 ” and k stands for first order-pseudo rate constant. Figure 9d shows that 4% La-doped WO_3 has highest rate constant and it exhibit maximum degradation efficiency (Viswanathan 2018) The value of R^2 is significantly larger than 0.95, demonstrating that the linear regression was the most appropriate analysis for this data.

4.2 Reusability study

Photo catalysts must be stable and reused for waste water treatment that is economically feasible and reused for a long time (Sharif et al. 2021; Ashraf 2023). In this study, the cyclic test of MB degradation was performed for investigation of stability and optimal photo catalyst reusability i.e. 4% La-doped WO_3 . The catalyst washed with distilled water many times and then dried for three hours at 80°C before being used in other experiment (Rafique et al. 2020). Figure 9f. depicts the observation of five consecutive cycles of MB degradation. After five consecutive cycles, there was a small change in photocatalytic efficiency of MB decomposition (94–74.5%) subsequent use of 4% La-doped WO_3 . The results show that the fabricated 4% La-doped WO_3 photocatalyst is stable, long-lasting and reusable.

4.3 Scavenger analysis

Scavenger analysis were carried out to depict the active species accountable for MB degradation (Areej 2023). This experiment is performed by adding 1 mmol ethylenediaminetetraacetate (EDTA), 1 mmol tert-Butyl alcohol (t-BuOH) and 1 mmol benzoquinone (BQ) has been used to trap h^+ , O_2^- and OH respectively that formed in the reaction mixture (Zou et al. 2021). Degradation efficiency decreased upto 39% by adding EDTA scavengers in reaction process. The concentration of MB as a function of degradation % in the absence and presence of several scavengers shown in Fig. 10. EDTA, t-BuOH and BQ were slow down the degradation rate demonstrating h^+ , O_2^- and $\cdot OH$ all have significant impact on photo catalytic degradation (Munawar et al. 2023a).

4.4 Mechanism of photocatalytic degradation

The mechanism of degradation can be explained in such a way that by falling light on the surface of the photocatalyst, valence band (VB) electrons move to the conduction band (CB) and holes remain in VB as seen in Fig. 11 (Sardar et al. 2023). When holes that remains in the VB combine with molecules of water molecules, they produced hydroxyl radical (OH^-) and O_2^- radicals formed. When electron combines with O_2 molecule to form superoxide radicals O_2^- thus the degradation of MB occur (Kannan et al. 2022). O_2^- and OH^- take part in the decomposition of dye molecules thus carbon dioxide and water are produced. (Kannan et al. 2021). Additionally, the excited electron was trapped by the doping of La, which slows down the rate of recombination (Nachimuthu et al. 2022).

4.5 COMOSL simulation

A theoretical analysis has been performed to correlate the findings from the experimental analysis. For this purpose, a 2D model of COMSOL Multiphysics has been used as shown in (Fig. 12). The internal borders of the model take into account the CBC while opposite dimensions of the model use PBC to simulate the existence of analogous unit cells across the opposite sides of the unit cell. Scattering Boundary Conditions (SBC) ensures the incoming radiations of electromagnetic from the 2D model power port (Tahir et al. 2020). Various boundary conditions are applied to simulate the experimental conditions. The designed model is excited with near-infrared to UV-Vis radiation using the input port. The radiations must be adequately dispersed and this is ensured by the scattering boundary condition (SBC) (Ashraf 2023).

In contrast to the interior boundaries of designed model, which utilize continuous boundary conditions (CBC), the opposite sides of the model use periodic boundary conditions (PBC). These boundary conditions' equations are provided below:

$$E_{dst} = E_{src} \exp(-jk \cdot (r_{dst} r_{src})) \quad (7)$$

Continuous boundary conditions

$$(n \times (H_1 - H_2))_z = 0, (n \times (E_1 - E_2))_z = 0 \quad (8)$$

Fig. 10 Effect of various scavengers on 4% La-doped WO₃ NPs

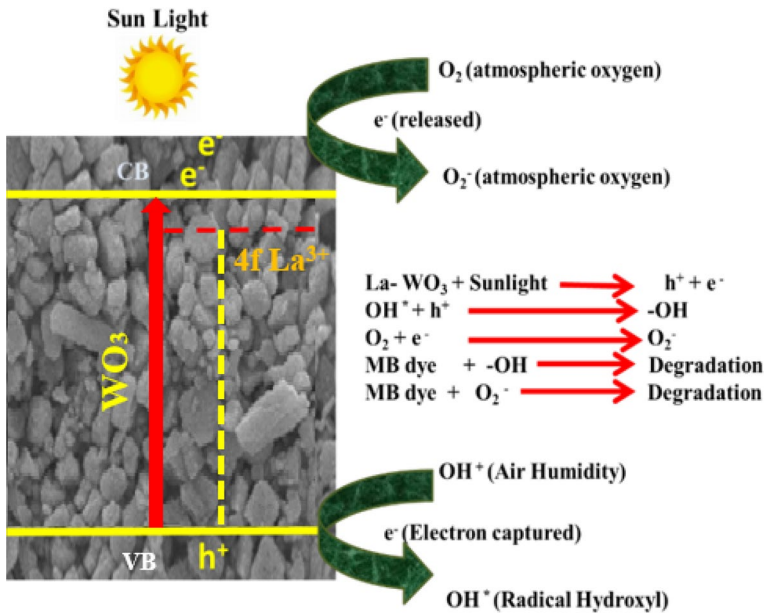
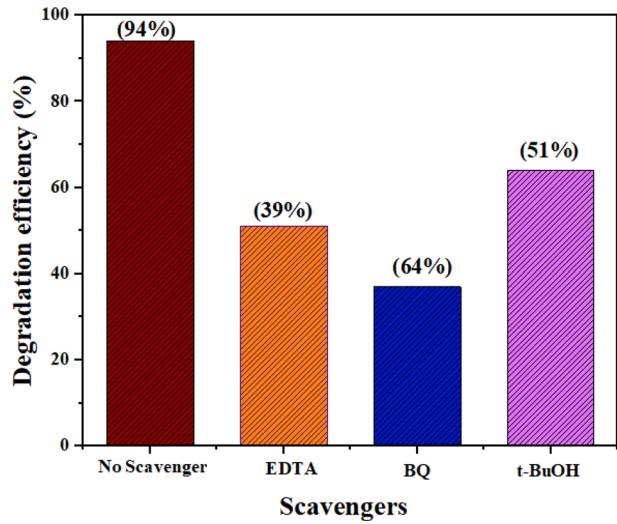


Fig. 11 Photo-catalytic Mechanism of La doped WO₃ nanoparticles

Scattering boundary condition (SBC)

$$n \times (\nabla \times A_z) - jkA_z = -jk(1 - k.n)A_{0z} \exp(-jk.r), A = EorH \tag{9}$$

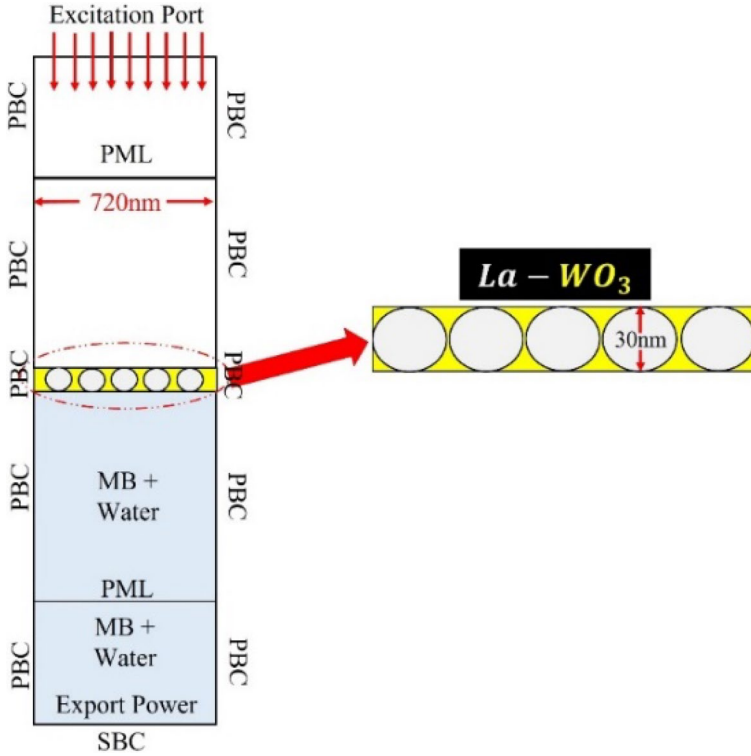


Fig. 12 Schematic geometry of 2D model of COMSOL Multiphysics

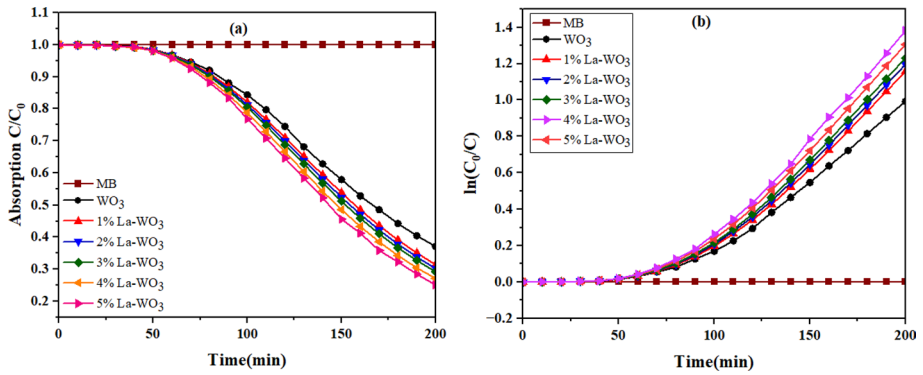


Fig. 13 **a** demonstrates the improvement in absorption of pure and La-doped WO_3 NPs & **b** Represents the degradation of MB by using pure and La- doped (1% to 5%) WO_3 NPs

Port

$$s = f (E - E_1) \cdot \frac{E_1}{E_1 \cdot E_2} \tag{10}$$

First, the model is meshed and the simulation utilized WO_3 particles with an experimental NPs size of 30 nm. WO_3 nanoparticles dissolved in an MB solution for 200 min during the simulation. To achieve the best results, the wavelength varies from 300 to 1000 nm having 1 nm step size. The results displayed in Fig. 13a demonstrate the beneficial effects of La- WO_3 presence for light absorption. Higher photocatalytic efficiency is due to improved absorption, which also contributes to the efficient inclusion of photo generated electron/hole pairs. The experiments showed equivalent results.

5 Conclusion

In this work, a simple hydrothermal method has been used for the preparation of WO_3 and La doped WO_3 nanoparticles. The calculated band gaps for pure WO_3 and La doped (1, 2, 3, 4 and 5%) WO_3 NPs were 2.81, 2.7, 2.6, 2.49, 2.23 eV, and 2.39 eV respectively. PL analysis showed that the recombination rate of 4% La-doped WO_3 is lowered and it exhibits maximum photocatalytic degradation efficiency. XRD analysis showed that the crystalline size of WO_3 and 4% La-doped WO_3 NPs is 30 nm and 11 nm respectively. SEM images further showed that the particle size decreased as the dopant concentration increased. Furthermore, 4% La- WO_3 NPs show 94% degradation of MB dye within 180 min that promotes its stability. Employing several scavengers, a trapping experiment was conducted and the results show that h^+ , $\cdot\text{O}_2^-$ and $\cdot\text{OH}$ were significantly involved in the breakdown of MB. COMSOL simulation shows that the photocatalytic activity of 4% La-doped WO_3 nanoparticles is higher than undoped WO_3 , exhibit the efficient and correlation factor with experimental results. In comparison to various concentrations, 4% La-doped WO_3 NPs behave as an optimal photo catalyst for the treatment of industrial wastewater.

Acknowledgements The researchers wish to extend their sincere gratitude to the Deanship of Scientific Research at the Islamic University of Madinah for the support provided to the Post-Publishing Program.

Author Contributions AY: writing—original draft, data curation, methodology, validation, project administration. TI, SA and AA: conceptualization, supervision.

Funding Deanship of Scientific Research at the Islamic University of Madinah.

Data availability All data generated or analyzed during this study are included in this published article.

Declarations

Competing interests The authors declare that they have no competing interests.

References

- Ahmed, S.N., Haider, W.: Heterogeneous photocatalysis and its potential applications in water and wastewater treatment: a review. *Nanotechnology* **29**(34), 342001 (2018)
- Al-Nuaim, M.A., Alwasiti, A.A., Shnain, Z.Y.: The photocatalytic process in the treatment of polluted water. *Chem. Pap.* **77**(2), 677–701 (2023)
- Antony, A.J., et al.: Enhancing the visible light induced photocatalytic properties of WO_3 nanoparticles by doping with vanadium. *J. Phys. Chem. Solids* **157**, 110169 (2021)

- Areej, F., Munawar, T., Mukhtar, F., Nadeem, M.S., Akbar, U.A., Hakeem, A.S., Iqbal, F.: Synthesis and characterization of rGO-supported Mo/Cu dual-doped NiO nanocomposite for the elimination of dye pollutant. *Appl Nanosci* (2023). <https://doi.org/10.1007/s13204-023-02786-6>
- Ashraf, M., Iqbal, T., Masood, A., Masood, N., Abdella, F.I., El-Sofany, W.I., Mansha, M.S.: Experimental and theoretical verification of WO₃ based nanocomposites for their application as efficient photo catalyst for treatment of industrial wastewater. *J Inorg Organometal Polym Mater* (2023). <https://doi.org/10.1007/s10904-023-02705-w>
- Ashraf, M., et al.: Experimental and theoretical verification of WO₃ Based nanocomposites for their application as efficient photo catalyst for treatment of industrial wastewater. *J Inorg Organometal Poly Mater* (2023). <https://doi.org/10.1007/s10904-023-02705-w>
- Azimi, A., Azari, A., Rezakazemi, M., Ansarpour, M.: Removal of heavy metals from industrial wastewaters: a review. *Chem Bio Eng Rev* **4**(1), 37–59 (2017)
- Chandekar, K.V., Shkir, M., Al-Shehri, B.M., AlFaify, S., Halor, R.G., Khan, A., Hamdy, M.S.: Visible light sensitive Cu doped ZnO: facile synthesis, characterization and high photocatalytic response. *Mater Char* **165**, 110387 (2020)
- Chaudhry, F.N., Malik, M.F.: Factors affecting water pollution: a review. *J. Ecosyst. Ecography* **7**(1), 225–231 (2017)
- Chen, X., et al.: Visible light photocatalytic degradation of dyes by β -Bi₂O₃/graphene nanocomposites. *J. Alloy. Compd.* **649**, 872–877 (2015)
- Chen, D., et al.: Photocatalytic degradation of organic pollutants using TiO₂-based photocatalysts: a review. *J. Clean. Prod.* **268**, 121725 (2020)
- Deshmane, V.G., Abrokwhah, R.Y., Kuila, D.: Mesoporous nanocrystalline TiO₂ supported metal (Cu Co, Ni, Pd, Zn, and Sn) catalysts: effect of metal-support interactions on steam reforming of methanol. *J Mol Catal A Chem* **408**, 202–213 (2015)
- Fatima, S., Munawar, T., Nadeem, M.S., Mukhtar, F., Khan, S.A., Koc, M., Iqbal, F.: Boosted natural sunlight driven photodegradation of organic dyes using rGO anchored Pr/Cu dual-doped ZnO nanocomposite: Characterization and mechanistic insight. *Opt Mater* **136**, 113397 (2023)
- Govindaraj, T., Mahendran, C., Chandrasekaran, J., Manikandan, V.S., Shkir, M., Massoud, E.E.S., Gedi, S.: Effect of incorporation of La into WO₃ nanorods for improving photocatalytic activity under visible light irradiation. *J Phys Chem Solids* **170**, 110908 (2022)
- Han, X., et al.: Preparation and photocatalytic performances of WO₃/TiO₂ composite nanofibers. *J. Chem.* **2020**, 1–12 (2020)
- Haseena, M., et al.: Water pollution and human health. *Environ Risk Assess Remediat.* **1**(3), 16–19 (2017)
- He, G.H., He, G.L., Li, A.J., Li, X., Wang, X.J., Fang, Y.P., Xu, Y.H.: Synthesis and visible light photocatalytic behavior of WO₃ (core)/Bi₂WO₆ (shell). *J Mol Catal A Chem* **385**, 106–111 (2014)
- Iqbal, T., Ashraf, M., Masood, A.: Simple synthesis of WO₃ based activated carbon co-doped CuS composites for photocatalytic applications. *Inorg Chem Commun* **139**, 109322 (2022)
- Iqbal, T., Ashraf, M., Masood, A.: Simple synthesis of WO₃ based activated carbon co-doped CuS composites for photocatalytic applications. *Inorg. Chem. Commun.* **139**, 109322 (2022b)
- Jabbar, Z.H., Graimed, B.H.: Recent developments in industrial organic degradation via semiconductor heterojunctions and the parameters affecting the photocatalytic process: a review study. *J Water Process Eng* **47**, 102671 (2022)
- Jeevitha, G., Abhinayaa, R., Mangalaraj, D., Ponpandian, N.: Tungsten oxide-graphene oxide (WO₃-GO) nanocomposite as an efficient photocatalyst, antibacterial and anticancer agent. *J Phys Chem Solids* **116**, 137–147 (2018)
- Kannan, K., Radhika, D., Nesaraj, A.S., Sadasivuni, K.K., Krishna, L.S.: Facile synthesis of NiO-CYSO nanocomposite for photocatalytic and antibacterial applications. *Inorg Chem Commun* **122**, 108307 (2020)
- Kannan, K., Radhika, D., Gnanasangeetha, D., Krishna, L.S., Gurushankar, K.: Y³⁺ and Sm³⁺ co-doped mixed metal oxide nanocomposite: Structural, electrochemical, photocatalytic, and antibacterial properties. *Appl Surf Sci Adv* **4**, 100085 (2021)
- Kannan, K., Radhika, D., Kasai, R.D., Gnanasangeetha, D., Palani, G., Gurushankar, K., Shim, J.: Facile fabrication of novel ceria-based nanocomposite (CYO-CSO) via co-precipitation: Electrochemical, photocatalytic and antibacterial performances. *J Mol Struct* **1256**, 132519 (2022)
- Khan, M.I., Fatima, N., Shakil, M., Tahir, M.B., Riaz, K.N., Rafique, M., Mahmood, K.: Investigation of in-vitro antibacterial and seed germination properties of green synthesized pure and nickel doped ZnO nanoparticles. *Phys B: Condens Matter* **601**, 412563 (2021)
- Koe, W.S., et al.: An overview of photocatalytic degradation: photocatalysts, mechanisms, and development of photocatalytic membrane. *Environ. Sci. Pollut. Res.* **27**, 2522–2565 (2020)

- Lan, X., Wang, L., Zhang, B., Tian, B., Zhang, J.: Preparation of lanthanum and boron co-doped TiO₂ by modified sol–gel method and study their photocatalytic activity. *Cataly Today* **224**, 163–170 (2014)
- Li, J., Feng, J., Yan, W.: Excellent adsorption and desorption characteristics of polypyrrole/TiO₂ composite for methylene blue. *Appl Surf Sci* **279**, 400–408 (2013)
- Martínez, D.S., Martínez-De La Cruz, A., Cuéllar, E.L.: Photocatalytic properties of WO₃ nanoparticles obtained by precipitation in presence of urea as complexing agent. *Appl Catal A General* **398**(1–2), 179–186 (2011)
- Maryam, I., Iqbal, T., Afsheen, S., Ali, A.M.: Synthesis and characterization of ta-doped WO₃ nanomaterials for their application as an efficient photocatalyst. *J Inorg Organometal Poly Mater* (2023). <https://doi.org/10.1007/s10904-023-02776-9>
- Maryam, I., et al.: Synthesis and characterization of ta-doped WO₃ nanomaterials for their application as an efficient photocatalyst. *J Inorg Organometal Poly Mater* (2023). <https://doi.org/10.1007/s10904-023-02776-9>
- Masood, A., Iqbal, T., Ashraf, M., Nazir, A., Ali, F., Ranjha, Q.A., Galal, A.M.: Synthesis and characterization of cadmium doped zinc oxide nanoparticles for visible light driven catalytic removal of MB and RhB Dye: experimental and computational analysis. *J Inorg Organometal Poly Mater* (2023). <https://doi.org/10.1007/s10904-023-02618-8>
- Mohammed Harshulkhan, S., Janaki, K., Velraj, G., Sakthi Ganapthy, R., Nagarajan, M.: Effect of Ag doping on structural, optical and photocatalytic activity of tungsten oxide (WO₃) nanoparticles. *J Mater Sci Mater Electron* **27**(5), 4744–4751 (2016)
- Munawar, T., Sardar, S., Mukhtar, F., Nadeem, M.S., Manzoor, S., Ashiq, M.N., Iqbal, F.: Fabrication of fullerene-supported La₂O₃-C₆₀ nanocomposites: dual-functional materials for photocatalysis and supercapacitor electrodes. *Phys Chem Chem Phys* **25**(9), 7010–7027 (2023)
- Munawar, T., Fatima, S., Nadeem, M.S., Mukhtar, F., Akbar, U.A., Hakeem, A.S., Iqbal, F.: Tunability of physical properties of NiO by the introduction of rare earth metal (Y, Ho) dual doping for natural sunlight-driven photocatalysis. *J Mater Sci Mater Electron* **34**(7), 687 (2023)
- Murillo-Sierra, J.C., Hernández-Ramírez, A., Hinojosa-Reyes, L., Guzmán-Mar, J.L.: A review on the development of visible light-responsive WO₃-based photocatalysts for environmental applications. *Chem Eng J Adv* **5**, 100070 (2021)
- Mutahir, S., et al.: Synthesis and micromechanistic studies of sensitized bentonite for methyl orange and rhodamine-B adsorption from wastewater: experimental and DFT-based analysis. *Molecules* **27**(17), 5567 (2022)
- Nachimuthu, S., Thangavel, S., Kannan, K., Selvakumar, V., Muthusamy, K., Siddiqui, M.R., Parvathiraja, C.: Lawsonia inermis mediated synthesis of ZnO/Fe₂O₃ nanorods for photocatalysis–Biological treatment for the enhanced effluent treatment, antibacterial and antioxidant activities. *Chem Phys Lett* **804**, 139907 (2022)
- Paik, T., Cargnello, M., Gordon, T.R., Zhang, S., Yun, H., Lee, J.D., Murray, C.B.: Photocatalytic hydrogen evolution from substoichiometric colloidal WO_{3-x} nanowires. *ACS Energy Lett* **3**(8), 1904–1910 (2018)
- Pal, B., et al.: Hydrothermal syntheses of tungsten doped TiO₂ and TiO₂/WO₃ composite using metal oxide precursors for charge storage applications. *J. Alloy. Compd.* **740**, 703–710 (2018)
- Pang, H.F., Xiang, X., Li, Z.J., Fu, Y.Q., Zu, X.T.: Hydrothermal synthesis and optical properties of hexagonal tungsten oxide nanocrystals assisted by ammonium tartrate. *Phys Status Solidi a* **209**(3), 537–544 (2012)
- Quyen, V.T., Kim, J., Park, P.M., Huong, P.T., Viet, N.M., Thang, P.Q.: Enhanced the visible light photocatalytic decomposition of antibiotic pollutant in wastewater by using Cu doped WO₃. *J Environ Chem Eng* **9**(1), 104737 (2021)
- Rafique, M., Tahir, M.B., Irshad, M., Nabi, G., Gillani, S.S.A., Iqbal, T., Mubeen, M.: Novel Citrus aurantifolia leaves based biosynthesis of copper oxide nanoparticles for environmental and wastewater purification as an efficient photocatalyst and antibacterial agent. *Optik* **219**, 165138 (2020)
- Ren, G., Han, H., Wang, Y., Liu, S., Zhao, J., Meng, X., Li, Z.: Recent advances of photocatalytic application in water treatment: a review. *Nanomaterials* **11**(7), 1804 (2021)
- Sa-nguanprang, S., Phuruangrat, A., Karthik, K., Thongtem, S., Thongtem, T.: Tartaric acid-assisted precipitation of visible light-driven Ce-doped ZnO nanoparticles used for photodegradation of methylene blue. *J Aust Ceram Soc* **56**, 1029–1041 (2020)
- Sardar, S., Munawar, T., Mukhtar, F., Nadeem, M.S., Khan, S.A., Koc, M., Iqbal, F.: Fullerene triggered energy storage and photocatalytic ability of La₂O₃-ZnO@ C₆₀ core-shell nanocomposite. *Mater Sci Eng B* **288**, 116151 (2023)

- Sarojini, P., Leeladevi, K., Kavitha, T., Gurushankar, K., Sriram, G., Oh, T.H., Kannan, K.: Design of V_2O_5 blocks decorated with garlic peel biochar nanoparticles: a sustainable catalyst for the degradation of methyl orange and its antioxidant activity. *Materials* **16**(17), 5800 (2023)
- Sayed Abhudhahir, M.H., Kandasamy, J.: Photocatalytic effect of manganese doped WO_3 and the effect of dopants on degradation of methylene blue. *J Mater Sci Mater Electron* **26**(11), 8307–8314 (2015)
- Shandilya, P., Sambyal, S., Sharma, R., Mandyal, P., Fang, B.: Properties, optimized morphologies, and advanced strategies for photocatalytic applications of WO_3 based photocatalysts. *J Hazard Mater* **428**, 128218 (2022)
- Sharif, M.S., et al.: Photocatalytic, bactericidal and molecular docking analysis of annealed tin oxide nanostructures. *Nanoscale Res. Lett.* **16**(1), 1–16 (2021)
- Štengl, V., Bakardjieva, S., Murafa, N.: Preparation and photocatalytic activity of rare earth doped TiO_2 nanoparticles. *Mater. Chem. Phys.* **114**(1), 217–226 (2009)
- Tahir, M.B., Ahmad, A., Iqbal, T., Ijaz, M., Muhammad, S., Siddeeq, S.M.: Advances in photo-catalysis approach for the removal of toxic personal care product in aqueous environment. *Environ Dev Sustain* **22**, 6029–6052 (2020)
- Ullah, R., Dutta, J.: Photocatalytic degradation of organic dyes with manganese-doped ZnO nanoparticles. *J. Hazard. Mater.* **156**(1–3), 194–200 (2008)
- Villar, L., et al.: Testing thymol-based DES for the elimination of 11 textile dyes from water. *Separations* **9**(12), 442 (2022)
- Viswanathan, B.: Photocatalytic degradation of dyes: an overview. *Current Catal* **7**(2), 99–121 (2018)
- Weber, A.S., Grady, A.M., Koodali, R.T.: Lanthanide modified semiconductor photocatalysts. *Catal Sci Technol* **2**(4), 683–693 (2012)
- Wei, N., Cui, H., Song, Q., Zhang, L., Song, X., Wang, K., Tian, J.: Ag_2O nanoparticle/ TiO_2 nanobelt heterostructures with remarkable photo-response and photocatalytic properties under UV, visible and near-infrared irradiation. *Appl Catal B Environ* **198**, 83–90 (2016)
- Zhu, Xiyang, Zhang, Pan, Li, Bin, Qun, Hu., Wenli, Su., Dong, Lihui, Wang, Fan: Preparation, characterization and photocatalytic properties of La/WO_3 composites. *J Mater Sci Mater Electron* **28**, 12158–12167 (2017)
- Zhu, X., Zhang, P., Li, B., Hu, Q., Su, W., Dong, L., Wang, F.: Preparation, characterization and photocatalytic properties of La/WO_3 composites. *J Mater Sci Mater Electron* **28**, 12158–12167 (2017)
- Zou, R., et al.: CeO_2/CdS heterojunction decorated cotton fabric as a recyclable photocatalyst for efficient light driven degradation of methylene blue. *Cellulose* **28**, 11081–11096 (2021)

Publisher's Note Springer Nature remains neutral with regard to jurisdictional claims in published maps and institutional affiliations.

Springer Nature or its licensor (e.g. a society or other partner) holds exclusive rights to this article under a publishing agreement with the author(s) or other rightsholder(s); author self-archiving of the accepted manuscript version of this article is solely governed by the terms of such publishing agreement and applicable law.